Breakthrough adsorption study using activated carbon and molecular sieve for CO2 capture

Mohd Danish (danishmohd111@yahoo.com)
King Khalid University https://orcid.org/0000-0002-7321-2958
Vijay Parthasarthy
University of Petroleum and Energy Studies
Mohammed K. Al Mesfer
King Khalid University

Research Article

Keywords: Breakthrough CO2 uptake, Capacity utilisation factor, Biomass, Continuous fixed bed, Mass transfer zone

Posted Date: March 30th, 2021

DOI: https://doi.org/10.21203/rs.3.rs-323987/v1

Breakthrough adsorption study using activated carbon and molecular sieve for CO_2 capture

Mohd Danish[1, 2]. Vijay Parthasarthy[2]. Mohammed K. Al Mesfer[1]

[1]Chemical Engineering Department, College of Engineering, King Khalid University, Abha 61411 Kingdom of Saudi Arabia

[2]Chemical Engineering Department, University of Petroleum and Energy Studies, Dehradun, India

✉ danishmohd111@yahoo.com, +966 172419615

Abstract

The increased levels of carbon dioxide in the environment have incited the search of breakthrough technologies to lessen their impact on climate. The fixed bed CO_2 adsorption study has been carried out using two-grades of adsorbents from CO_2/N_2 feed. The molecular sieve 3Å and porous carbon prepared from low-cost date stone were used for the adsorption study. BET analyser and a scanning electron microscope were used to analyze the surface and morphological characteristics of activated carbons. The result of temperature, flow rate, initial carbon dioxide concentration levels in feed on breakthrough behaviour was analysed. The adsorption response was explored in terms of breakthrough and saturation points, CO_2 uptake, temperature profiles, effective column efficiency, usable bed height, utilization factor and length of mass transfer zone. The vastly steep breakthrough curves produced under different operating conditions reveals satisfactory utilisation of adsorbent capacity at breakthrough condition. The CO_2 uptake of 73.08 mg/g was attained having high effective column capacity of 0.938 at 298 K for synthesized activated carbon. The activated carbon AC-SY performs better with lessen L_{MTZ} of 1.20 cm and improved utilization factor of 0.97 at C_o=5 % and 298 K. The findings of study suggest that activated carbon developed from date stone is highly encouraging to capture CO_2 from CO_2/N_2 mixture using continuous fixed bed column.

Keywords Breakthrough CO_2 uptake . Capacity utilisation factor . Biomass . Continuous fixed bed . Mass transfer zone

Introduction

An increased level of CO_2 in the environment is seriously contributing to global warming. The most imperative problem of environment is apprehensive with the disturbing pace at which CO_2 atmospheric level is mounting (Rashidi and Yusuf 2016). The reachable CO_2-lessening technologies have the prospective to reduce the costs of CO_2 discharge in the atmosphere. The various recommended methods can be modified to prevailing plants banking on non-renewable source of fuel (MacDowell et al. 2010; Yang et al. 2008; Cohen et al. 2011) owing to the actuality that post-combustion CO_2 reduction is a realistic process. In post-combustion emissions, the adsorption is a leading technology to separate CO_2 (Valverde et al. 2011; Garcia et al. 2011). An adsorbent preferably captures CO_2 and, subsequently, regenerates to discharge CO_2 regardless the configuration of process (Alonso et al. 2010). An industrially obtainable porous materials were investigated widely to explore adsorption response to analyse the result of different parameters on capacity of adsorption (Al Mesfer and Danish 2018; Al Mesfer et al. 2018; Al-

Janabi et al. 2018; Shen et al. 2010; Lu et al. 2008; Shen et al. 2011). Several low cost- biomasses have been converted into activated carbons for CO_2 capture. Macadamia shell based biomass was utilized to synthesize activated carbons using microwave irradiation (Dejang et al. 2015). Investigator (Calvo-Munoz et al. 2016) synthesized a porous fibre and reported good CO_2 uptake of 1.3 mmol/g. The uptake of 9.09 mmol/g was predicted for adsorbent developed by coal treatment with potassium hydroxide (Toprak and Kopac 2017).

Two approaches: heat treatment with gaseous ammonia and activation with CO_2 were applied to produce carbon using olive residue (Plaza et al. 2019). Particularly at small pressure, the CO_2 capture capacity was found to rise in the presence of N_2 functionalities. The hydrothermal carbonisation technique was used to convert waste biomass into activated carbon for CO_2 separation (Hao et al. 2013). An elevated uptake equivalent to 1.45 mmol/g was attained at T= 0^{o}C using carbon developed by physical activation with CO_2. The effect of the activation means (Shahkarami et al. 2015) on the CO_2 capture using carbon prepared by pyrolysis of white wood was analyzed. The activation techniques were used to prepare the suitable adsorbent and highest CO_2 uptake of 1.8 mmol/g was predicted for an adsorbent developed treating by potassium hydroxide. Biomasses have been utilized to produce suitable adsorbent by means of activation by KOH (Coromina et al. 2016). A synthesized adsorbent with 1:2 ratio of hydrochar/KOH attributed to a CO_2 uptake of 5 mmol per g at 1 bar.

The carbon for enhanced CO_2 separation was synthesised from black locust applying the KOH induced activation (Zhang et al., 2016) and the capture capacity equivalent to 7.19 mmol/g at 0^{o}C was predicted. The chemical-activation technique with KOH was used to develop the carbon from wheat flour for separation of CO_2 (Hong et al. 2016) and 5.70 mmol CO_2 per g was adsorbed at 0^{o}C with a 1:3 proportion of C/KOH. The wheat bran incineration was evaluated to prepare ash and corresponding pellets, and 0.07 mmol/g CO_2 uptake was described using ash pellets at a temperature of 25^{o}C (Lira-Zuniga et al. 25). The preparation using KOH and thereafter, the carbonisation of waste pomegranate peel was carried out for CO_2 capture (Serafin et al. 2017) and a surface assimilation capacity of 1.25 mmol/g was predicted.

The various nuts based biomasses were utilized to produce carbon with potassium hydroxide with a prediction of 5.5 mmol/g separation capacity at 900^{o}C for peanut shells (Lewicka 2017). The result of methods of activation to synthesize carbon from olive stone for CO_2 separation was studied and recommended that subsistence of additional O_2 groups augmented the CO_2 adsorption capacity (Peredo-Mancilla et al. 2018). A significantly higher 101.7 mg CO_2/g of separation capacity was revealed at 30 ^{o}C for carbon produced from biomass (Zeng et al. 2018). The rapeseed and walnut mix was carbonised and, afterwards, treated with elevated temperature to develop carbon material (Davis and Kopac 2014). Also, walnut shell was utilized to produce carbon for developing the cartridge (Jahangiri et al. 2012). The porous carbonaceous materials were produced from different shells, and SEM and FTIR were used to analyze the structure of carbon (Patil et al. 2013). Porous carbons (Xia et al. 2016) were produced from walnut shells and KOH is identified as one of the approving agent for carrying out the activation. Researchers (Mataji and Khoshandam 2014) synthesised porous adsorbent from walnut shell, and investigated the separation ability of C_6H_6 by treating with $ZnCl_2$/H_3PO_4. The fixed bed CO_2 capture from CO_2/N_2 feed was investigated using porous carbon produced from walnut shell with a prediction 1.58 mmol/g separation capacity at 293 K (Almesfer

2020). The chemical activation technique (Banat et al. 2003) was used to synthesis activated carbon from raw date pits with impregnation of 30 wt% KOH and 123.1 mg/g separation capacity was attained. Two series of carbons were synthesized from date stones by steam activation (Belhachemi et al. 2009) and it was found that data pits can be utilized to produce activated carbon with good porosity and customized O_2 surface groups. An extensive review on utilizing data stone as adsorbent for aqueous /gaseous feed was carried out and preparation technique of activated carbon has been described (Daniel et al. 2012). The date seeds were converted into activated carbon by physical activation for CO_2 capture using micro calorimeter and capacity of 141.14 mg/g was reported (Ogungbenro et al. 2017). Enormous quantity of date stone based biomass is economically available in Kingdom of Saudi Arabia. There are very few studies in the literature about the synthesis of activated carbon from data stone and even fewer studies for CO_2 capture using fixed bed column to best our knowledge. The novelty of the current investigation is to produce porous activated carbon from date stone for CO_2 capture and comparing the performance with molecular sieve 3Å (MS 3Å) using fixed bed column. The performance of CO_2 capture was determined in terms of breakthrough curves, CO_2 uptake, effective column efficiency, usable bed height, temperature profiles, L_{MTZ} and f using temperature, feed rate and initial CO_2 level in feed as operating variables.

Material and Methods

Materials

The commercially available MS-3Å with average diameter of 1.60 mm was procured from Sigma-Aldrich. The date stones based biomass were collected from the local date shops. These collected date stones were washed with water several times to remove foreign impurities and overnight oven drying of biomass was carried out at 150ºC. The LC grinder (DLC-36250) was employed for grinding and milling purpose. The milled date stone particles were then passed through 4 mm screen (BS series). The particles are stored in air-proof containers for further use.

Experimental unit

Fixed bed experimental (UOP 15) procured from ARMFIELD, U.K., utilized for study has been depicted (Fig.1). The column was filled with adsorbents upto the effective length of 23 cm. The column (SS) is jacketed and permits hot water flow to accomplish the requisite temperature with the aid of water circulator. Flow controllers F_1 and F2 measure and control the flow of N_2, CO_2 that enters the column from bottom-side. The third mass flow controller F3 manages the CO_2 flow to IR detector. The IR detector is used to measure the CO_2 concentration at the bed outlet. Six thermocouples are located along the non-radial direction of the column to study temperature variations at different positions.

Procedure

Feed consisting of preset concentration levels made up of CO_2 and N_2 enters the column from bottom side as per the setup configuration. The mass flow controllers (F1 for N_2 - flow and F2 for CO_2 - flow) control the required feed flows. A heating jacket equipped with control console controls the requisite temperature with the help of PID controller. The column exit concentration C is regularly recorded at regular interval of 30 s using an IR sensor. Also, the uncertainty analysis (error analysis) was performed for all the measuring instruments. The measurement errors of

F1, F2, and F3 controllers along with temperature measurement were determined. A summary of uncertainty analysis of all the measurements is depicted in Table 1. The uncertainty in the measurement of temperature is estimated as ± 0.15 K. The controllers F1 (N_2 flow) and F2 (CO_2 Flow) add to an uncertainty of ±0.04 slpm and ±0.02 slpm, respectively. The uncertainty in the measurement of feed flow to IR sensor using mass flow controller F3 found to be equal ±0.01 lpm.

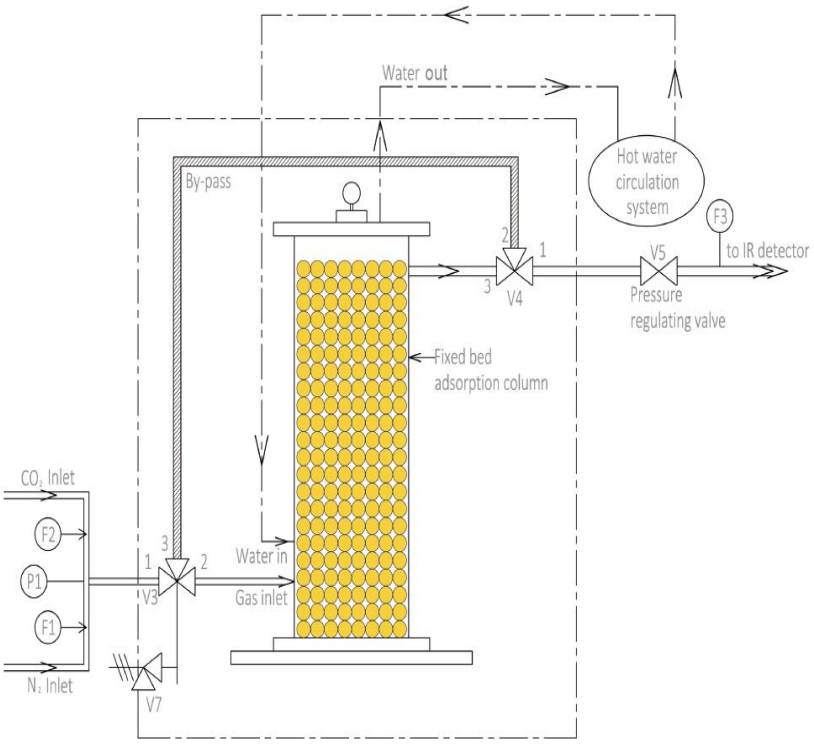

Fig.1 Fixed bed column

Table 1 Uncertainty analysis of all measuring instruments

Variable (u)	Sensor type	Uncertainty (δu)
N_2 flow rate (Slpm)	F1	±0.04
CO_2 flow rate (Slpm)	F2	±0.02
IR flow rate (Slpm)	F3	±0.01
Temperature (K)	Thermocouple type-K	±0.15

Physical Activation

The MS 3Å used for comparative purpose has been shown in Fig. 2a**.** Physical activation of date based biomass to prepare the activated carbon (AC-SY) was conceded with the help of a tubular furnace (Model: OTF-1200 X). The furnace consists of 3-zones that can be used to control dissimilar temperatures at the same time span. A known

sieved date stone weight was placed inner side the tube of furnace and afterwards, the temperature was raised at 10°C/min with a N_2 flow equal to 150 ml/min to accomplish the needed 600°C. The N_2 has been constantly maintained for an extra 2 hr for carbonisation. After that, the N_2 flow was closed and CO_2 flow allows constantly for 2 hrs at 600°C to develop desired carbon (AC-SY). The collected date stones and synthesised porous activated carbons are depicted in Fig. 2b – c. There is considerable reduction in adsorbent size after the activation. The produced AC-DS of size range: – 1.7 mm + 1.0 mm were chosen for the investigation.

Fig. 2 Date stone based biomass and activated carbon: **(a)** MS 3Å. **(b)** Date stone after oven drying. **(c)** Activated carbon AC-SY

Result and Discussion

Surface and morphological characterizations

The activated carbons (AC-SY) were characterised using NovaWin (Quantachrome) analyser for surface with 573 K outgas temperature. The analysis period was 88.3 min and N_2 was supplied for analysis purpose. The surface characterisation results for AC-SY and MS 3Å has been shown in Table 2. The single point surface area of 848.27 m^2/g was obtained for synthesised activated carbon. The pore volumes equal to 0.45 cm^3/g and 0.22 cm^3/g were observed for AC-SY and MS 3Å, respectively. The pore radius of activated carbon is significantly larger compared to that o molecular sieve. Largely, the adsorbents are vastly porous materials. The sorption takes place mostly either at definite sites within the particles or on the pore walls.

Table 2 Surface characterizations of MS-3Å and AC-SY

Adsorbent characteristics	MS-3Å	AC-SY
Single point surface (m^2/g)	25.04	848.27
Langmuir surface area (m^2/g)	46.21	956.87
Pore volume (cm^3/g)	0.22	0.45
Pore size (Å)	1.83	22.68

The surface morphology of AC-SY and MS 3Å was analysed by the SEM (Model: Quanta 250-FEI, Japan). The structural images have been depicted in Fig. 3a for MS 3^A and Fig. 3b for AC-SY. The numerous pores can be visualized and the pores almost distributed all over the structure, as presented in Fig. 3b with 1200 x level and Fig. 3a 1000 x level for MS 3Å. The very regular and high density pore structures are especially effective for CO_2 separation.

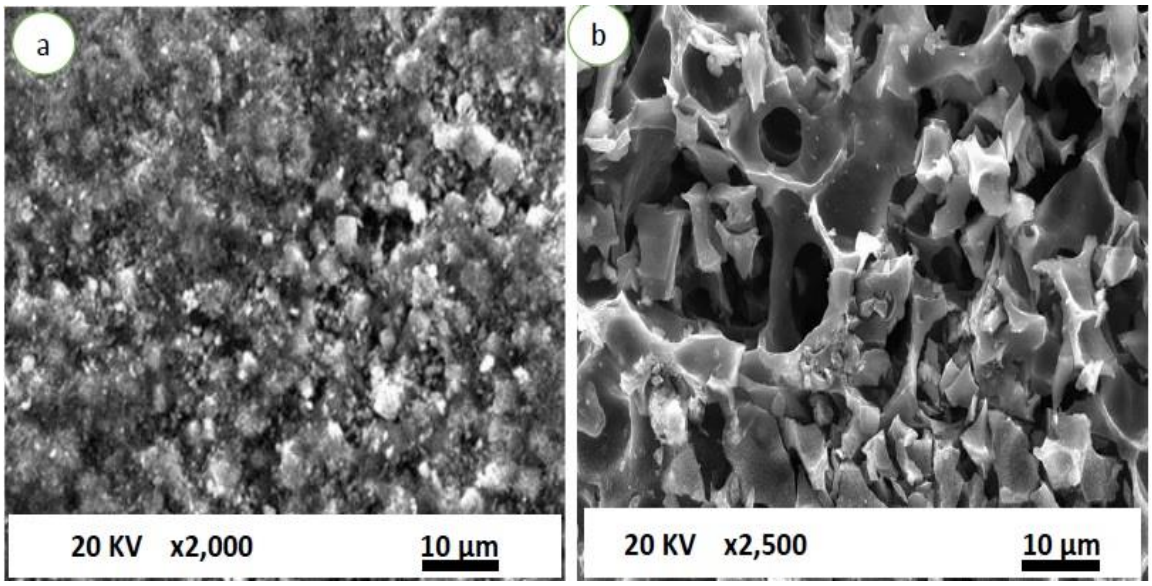

Fig.3 Morphological characteristics of adsorbents used for CO2 capture: **(a)** MS-3Å **(b)** AC-SY

The thermogravimetric analyzer (NETZSCH:TG209 FI Libra) was used to studty the thermal stability of the . The dependance of TG (%) and DTG (% change/min) on temperature has been presented in **Fig.4** for date stone base biomas. A sample mass 18.43 mg was heated upto 900 ^oC at a heating rate of 20 ^oC/min under N_2 purge rate of 20 ml/min with protective gas flow rate of 10 ml/min. The proximate analysis determined the weight loss as function of temperature. The derivative weight loss signifies the temperature at which the weight loss is more apparent and it is more beneficial approach to determine optimum condition of tempertaure and time. The change of TG(%) on temperature for porous activated carbon has been depicted in **Fig.5**.

An X-ray diffractometer (PANalytical X'Pert Pro) was used to analyze the components of deveopled activated carbon AC-DS. The X-ray patterns was measured in the scan range of 2θ= 0-100^o as shown in **Fig.6**. The occurance of broad peaks signifies the amorphous nature of produced activated carbon AC-DS. This is desired property of activated carbon for adsorption of CO_2. Three diffraction peaks at 2θ= 23.96^o, 45.34^o and 87.56^o are visualized from activated carbon material which corresponding to the peaks of amorphous carbon.

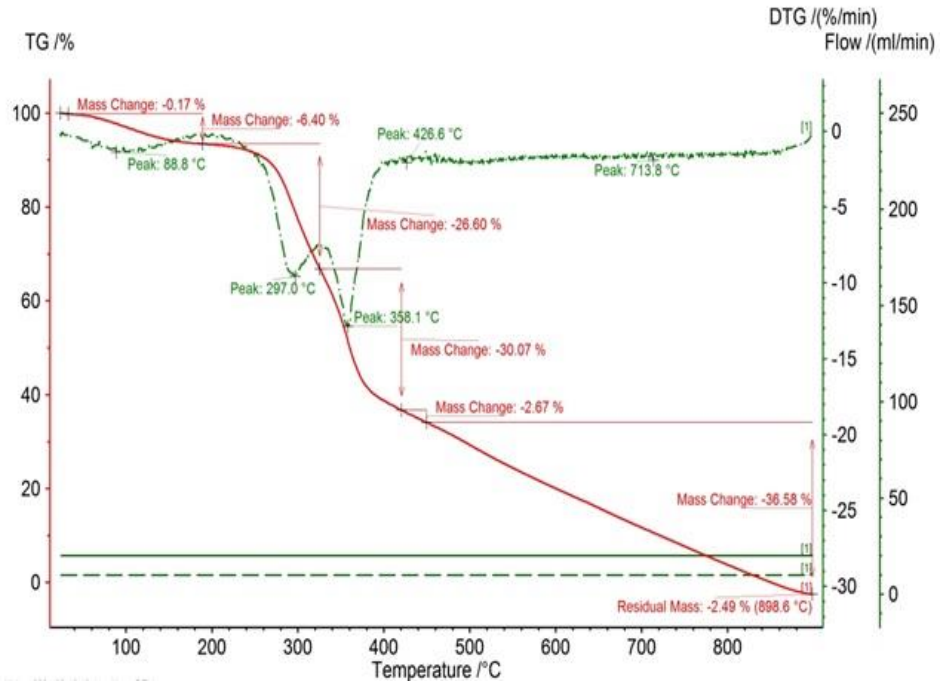

Fig.4 Thermogravimetric analysis curve of DS showing mass change and DGT

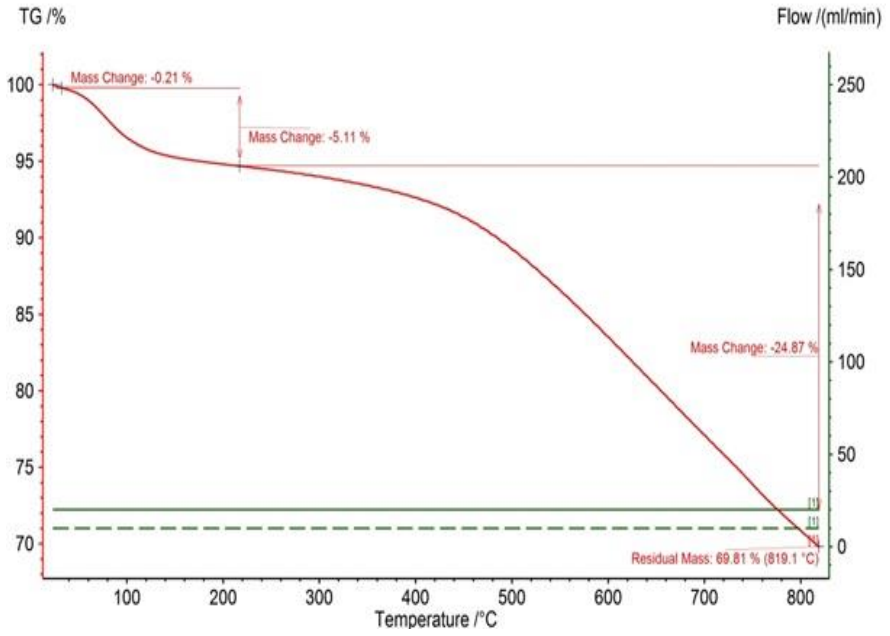

Fig.5 Thermogravimetric analysis curve of AC-SY showing mass change

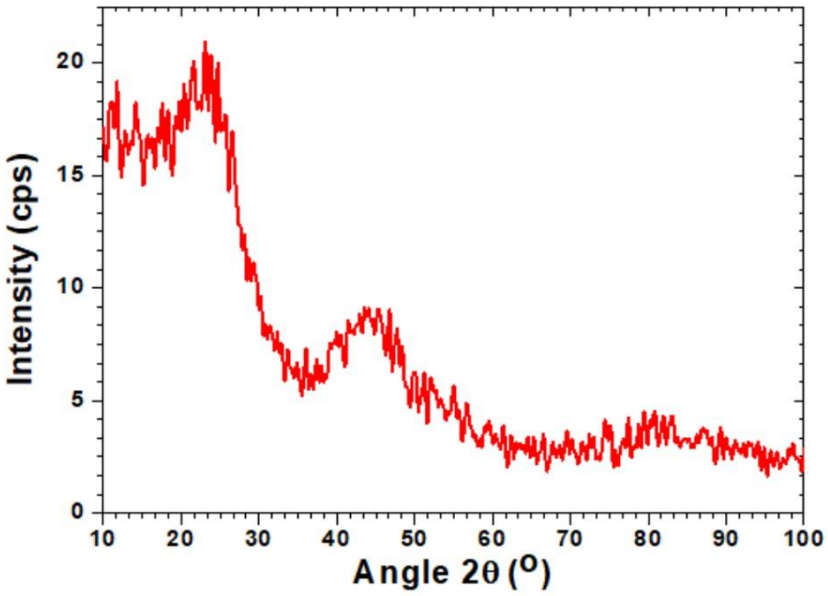

Fig.6 XRD analysis of date stone based activated carbon AC-SY

Breakthrough analysis

The N_2/CO_2 factual feed rates are calculated in terms of slpm and measured by mass flow controllers F1 and F2. The experiments were carried out at a feed rate of 4 lpm with a predetermined 5% CO_2 concentration level. The pressure of system was preset at a value of 1.25 bars (absolute) The breakthrough curves produced at different temperature for MS 3 Å (Mass, m_{ad}: 230 g) have been depicted in **Fig. 7a**. The breakthrough span of 417 s has been determined with a saturation period of 513 s at 298 K. The breakpoint and exhaustion periods reduced to 388 s and 459 s, respectively with an increased temperature to 308 K. The breakthrough time reduces to 250 for MS 3Å with increased temperature at 318 K. The saturation and breakthrough periods of 210 s and 283 s have been determined at 328 K. The lengthy breakthrough or exhaustion spans are constantly considered necessary for the increased adsorption under constant operating conditions. In general, the extended breakthrough period at lower temperatures suggests increased uptake of CO_2.

The breakthrough curves for AC-SY (Mass, m_{ad}: 150 gm) generated at different temperature have been shown in **Fig.7b**. The breakthrough period to a large extent relies on the temperature at which the adsorption occurs. Generally, the time it takes to reach 5% of the maximal concentration is called breakthrough time and then column must be regenerated for better effective column efficiency. The prolonged breakthrough and saturation periods attributed to reduced temperature at 298K. The extended breakthrough periods of 1524 s were attained at 298 K. The breakthrough and exhaustion (or saturation) periods reduced to 1265 s and 1348 s, respectively with an increased temperature to 308 K. The conditions of breakthrough and saturation appears early with a time periods of 1059 s and 1138 s at an increased temperature of 318 K. The highest studied 328 K temperature credited to breakthrough and exhaustion periods of 900 s and 958 s, respectively. The longer breakthrough and exhaustion periods have been

realized for AC-SY relative to MS 3Å under constant value of T. The breakthrough curves produced for AC-SY are comparatively steeper compared to that obtained for MS 3Å.

Also, the excellent utilization of the CO_2 uptake by bed is very well demonstrated by breakthrough curve which are vastly steep as evident for **Fig 7b**. The breakthrough curves generated for AC-SY are relatively steep compared to the breakthrough curves obtained for MS 3Å. The usage of desirable uptake corresponding to breakpoint condition is favoured for cost-effective capture of CO_2 from CO_2/N_2 mixture. Mass transfer zone (MTZ) thinness is dictated by the steepness of curves produced under various operating conditions. A small MTZ zone means that adsorption process occurs at a faster rate. The variations in molecular weight result in the occurrence of sorption. Also, several molecules held more firmly than others upon the adsorbent surface owing to polarity. In numerous instances, the adsorbate is held firmly and sufficiently to permit inclusive capture of CO_2 from feed with very small or no sorption of non-adsorbable. Indeed, steepness of all the curves in **Fig 7b** indicates that approximately alike utilisation of bed uptake of CO_2 upto the breakthrough. The bottom side layer is almost saturated and, largely, capturing occurs over a somewhat thin zone where the concentration varies speedily.

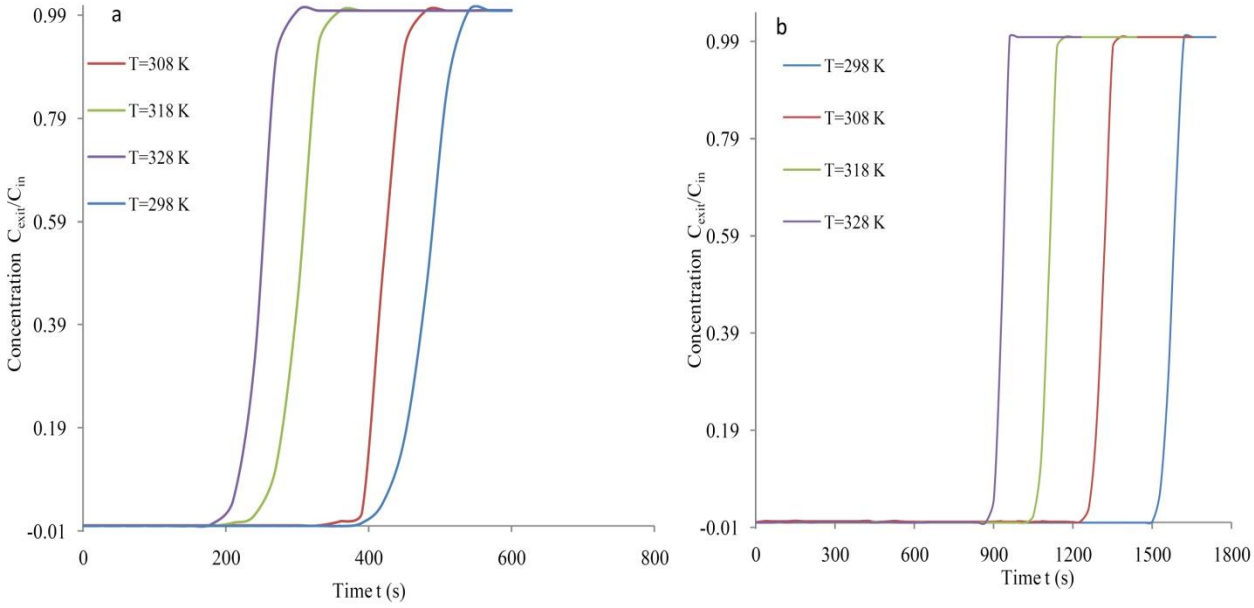

Fig.7 Adsorption response at various temperatures at F= 4 lpm, C_o=5%, **(a)** MS 3Å. **(b)** AC-SY

The dependence of feed flow on breakthrough pattern for MS 3Å was presented in **Fig. 8a**. The four different feed flows in the range of 2 to 5 lpm have been chosen at a preset 298 K temperature with 1.25 bars (absolute). The 2 slpm flow contributed to a breakthrough period of 650 s that is significantly lower than the period reported for AC-SY at the same feed rate. The breakthrough period was seen to reduce to 460 s with an increased feed flow to 3 slpm. The increased feed rate of 4 lpm attributed to reduced exhaustion and breakthrough spans of 311 s and 415 s with 298 K and C_o= 5%, respectively. The breakthrough time of 200 s was determined at highest studied feed rate of 5 lpm with T= 298K. Therefore, the exhaustion and breakthrough spell decline significantly with raised feed rate of CO_2/N_2 mixture.

The reliance of feed rates on breakthrough profiles generated for AC-SY was presented in **Fig. 8b**. The exhaustion and breakthrough periods rely remarkably on feed flows. The longer breakpoint and saturation periods of 2603 s and 2769 s were reached at 2 lpm feed rate. The period corresponding to C_{exit}= 0.05 C_{in} was observed to lessen from 2603 s to 1833 s with augmented feed flow from 2 lpm to 3 lpm with 298 K. Further, the breakthrough period declined to 1564 s with augmented 4 lpm feed flow. The smallest possible exhaustion and breakthrough periods of 1401 s and 1494 s were attained for activated carbon with a feed rate of 5 lpm. It was seen clearly that the prolonged breakthrough and exhaustion times are observed for activated carbon compared with MS 3Å at any predetermined feed rate.

The breakthrough curves produced at different feed rate for activated carbon are vastly steep as observed previously in **Fig.8b**. Also, the mass transfer zones depicted for breakthrough profiles are somewhat narrow, signifying the improved utilisation of bed capacity. The steepness of the S-shape breakthrough is especially noteworthy and vastly advantageous for the cost-effective CO_2 uptake. The C_{exit} increases rapidly equal to the curve ending at the condition the bed is well thought-out as ineffective and this happens when the breakthrough point is attained.

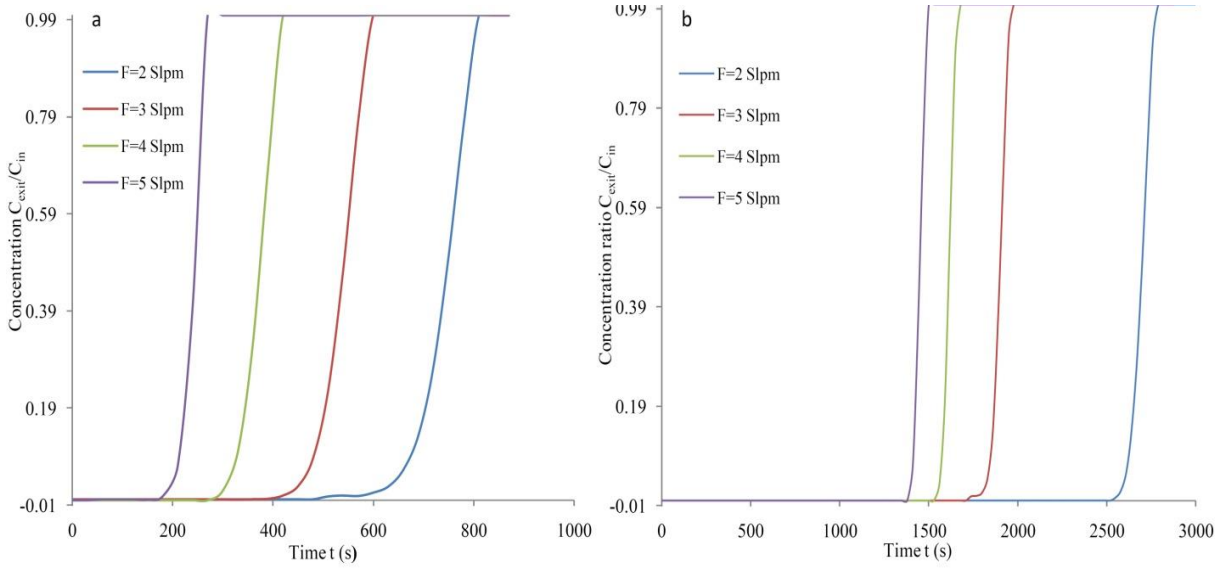

Fig.8 Adsorption response at various feed rates at T= 298 K, C_{in}=5%, **(a)** MS-3Å. **(b)** AC-SY

The reliance of C_{in} on the breakthrough profiles for MS 3Å was depicted in **Fig. 9a** under the same operating conditions of feed flow (F=4 slpm) and temperature (T=298K). The different concentrations of CO_2 in feed in the range of 2 - 5% were fixed with system pressures 1.25 bars (absolute). The concentration C_{in}= 2% in feed at 298 K attributed to an exhaustion and breakthrough periods of 420 s and 598 s with 4 lpm. The breakthrough and exhaustion spans were observed to lessen to 413 s and 543 s with increased level of initial adsorbable gas in feed at 3% level. The breakthrough period further reduced to 360 s with an increased Co to 4% with 298 K and 4 lpm. The

exhaustion period further diminishes to 380 s on increasing the CO_2 level at 5% under the fixed operating condition of feed flow. The prolonged breakthrough and exhaustion times are always required for increased CO_2 uptake.

The effect of initial CO_2 concentration level in feed on adsorption profiles at T= 298 K with F= 4 lpm has been presented in **Fig. 9b** for AC-SY. The breakthrough and exhaustion spell were observed to diminish with augmented CO_2 amount in feed. The lowest CO_2 concentration of 2% (vol.%) attributes to exhaustion and breakthrough times of 2422 s and 2280 s, respectively. The breakthrough time declined to 1884 s on raising the CO_2 level at 3% (vol.%). The same starting level of CO_2 contributes to a saturation period of 2005 s. The CO_2 concentration of 4% has shown early appearance exhaustion period of 1976 s. Highest adsorbate concentration of 5% in the feed predicted the time of breakthrough equivalent to 1695 s and demonstrates that the increased CO_2 quantity in the feed credited to the untimely appearance of exhaustion and breakthrough spans. It was obviously observed that exhaustion and breakthrough spans are longer for biomass based activated carbon compared to that determined for MS 3Å. The breakthrough span is proportional to the CO_2 loading and varies also reciprocally with feed concentration.

.

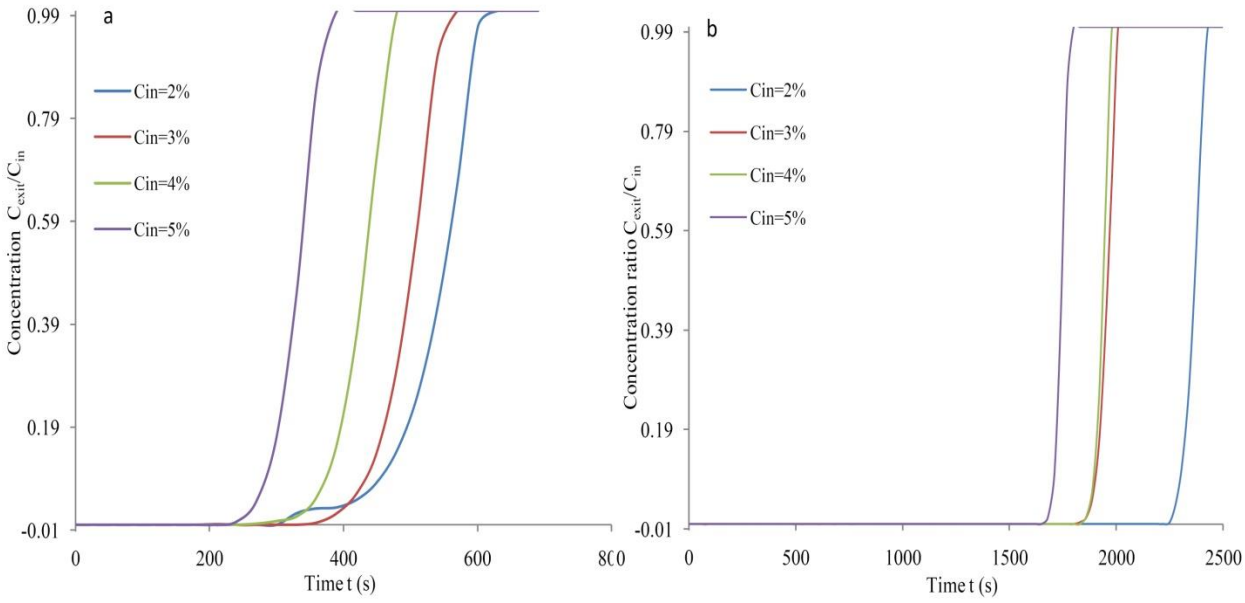

Fig.9 Adsorption response at various CO_2 level at F= 4 L/min, T= 298K, **(a)** MS-3Å. **(b)** AC-SY

Adsorption capacity and column efficiency

The CO_2 loading is approximated by applying mass balance. Utilising the breakthrough curves, the stoichiometric time (t_s) equal to the total uptake is usually determined (Monazam et al.2013) as:

$$t_s = \int_0^{\infty} \left(1 - \frac{C_{out}}{C_{in}}\right) dt \qquad (1)$$

Knowing t_s, the CO_2 uptake q of the bed may be evaluated (Serna-Guerrero and Sayari 2010) as:

$$q_s = \frac{F\, t_s C_{in}}{m_{ad}} \qquad (2)$$

Where, m_{ad}: mass of sorbent, F: feed rate, C: adsorbate concentration at time t, C_{in}: initial CO_2 level in feed.

Upto the breakthrough time t_b, the time equal to the usable capacity can be calculated as:

$$t_b = \int_0^t \left(1 - \frac{C_{out}}{C_{in}}\right) dt \qquad (3)$$

The corresponding column capacity until the breakthrough point can be calculated as:

$$q_b = \frac{F\, t_b C_{in}}{m_{ad}} \qquad (4)$$

The efficiency based on column capacity or faction of total column capacity that is effectively used:

$$\eta = \frac{q_b}{q_s} = \frac{\int_0^t \left(1 - \frac{C}{C_o}\right) dt}{\int_0^\infty \left(1 - \frac{C}{C_o}\right) dt} \qquad (5)$$

The length of adsorption column used upto the breakpoint Eq. (6):

$$L_b = \frac{t_b}{t_s} L \qquad (6)$$

Where L denotes the total bed height, an unutilized bed height can be determined as:

$$L_{ub} = \left(1 - \frac{t_b}{t_s}\right) L \qquad (7)$$

The adsorption performance for MS 3Å and AC-SY determined at different temperatures has been summarized as depicted in **Table 3**. The CO_2 uptake varies substantially with temperature for both types of adsorbents and alters negatively with temperatures. The maximal CO_2 uptake (q) of 63.18 mg/g was attained for AC-SY compared to a lower value of 13.83 mg/g for MS-3Å at 298 K with 4 lpm. The highest investigated temperature of 328 K contributed to a minimal capacity of adsorption and CO_2 uptake of 33.09 mg/g was determined for AC-SY. All the CO_2 capture system predicts a reduction in the uptake with an increased temperature. The prepared activated carbon contributed to higher effective column efficiency (η) as evident from the table 3. Also, the column efficiency (η) based on column capacity reported for synthesized carbon is considerably higher with a highest value 0.944 at 298 K. The fraction of total capacity is effectively used is 0.845 for MS 3 Å at 298 K. Significantly, higher efficiency of AC-SY indicates its feasibility for economical CO_2 capture. The effective column length (L) for the adsorption is fixed at 23 cm. Also, the bed length used upto the breakthrough point is 19.44 cm at 298 K for MS 3Å. The maximal bed length of 21.71 cm was used in case of AC-SY which is higher than reported for MS-3Å. Industrially, the essential cycle period and feed flow decides the size of adsorber. Applying a bed length of less than or equal to 12 cm is occasionally suggested to reduce adsorber height and drop in pressure, however empty needs more

regeneration energy and does not offer inclusive separation. It can be suggested that produced activated carbon performs very well and suitable for CO_2 separation from CO_2/N_2 feed.

Table 3 Adsorption characterizations at different temperatures (F= 4 slpm, C_{in}=5%)

	MS-3Å			AC-SY		
T(K)	q (mg/g)	η (fr.)	L_b (cm)	q (mg/g)	η (fr.)	L_b (cm)
298	13.83	0.845	19.44	63.18	0.944	21.71
308	11.64	0.834	19.18	50.60	0.938	21.57
318	8.24	0.746	17.16	44.45	0.931	21.41
328	6.74	0.742	17.07	33.09	0.939	21.60

The adsorption performance for MS-3Å and AC-SY determined at various feed flows has been summarized and depicted in **Table 4**. The CO_2 uptake varies positively and substantially with feed flow for both types of adsorbents. The maximal CO_2 uptake of 73.08 mg/g was determined for AC-SY at 298 K with 5 lpm. The lowest studied feed flow of 2 lpm contributed to a minimal capacity of adsorption and CO_2 uptake of 8.54 mg/g was for MS-3Å at the 298 K and C_{in}= 5%. The adsorption performance of developed activated carbon is reasonably higher at any fixed feed flow. The produced activated carbon contributed to higher effective column efficiency as evident from the Table 4. Also, the efficiency based on column capacity reported for synthesized carbon is considerably higher with a highest value of 0.940 at 2 lpm or 3 lpm with 298 K and C_{in}= 5%. The highest fraction of total capacity effectively used is 0.890 for MS-3Å with a feed flow of 2 lpm under the same condition of temperature and initial adsorbable gas level.

Table 4 Adsorption performances at various feed rates (T=298 K, C_{in}=5%)

	MS-3Å			AC-SY		
F (lpm)	q (mg/g)	η (fr.)	L_b (cm)	q (mg/g)	η (fr.)	L_b (cm)
2	10.33	0.890	20.47	54.30	0.940	21.62
3	11.52	0.776	17.80	57.55	0.940	21.62
4	10.73	0.749	17.23	65.43	0.939	21.60
5	8.54	0.746	17.16	73.08	0.938	21.57

In general, it was seen that effective column efficiency reduces marginally with increased feed flow of 2 to 5 lpm. Significantly, higher efficiency of AC-SY dictates its suitability for economical CO_2 separation from CO_2/N_2 mixture. The usable bed height upto the breakthrough reduces with increased feed flows for either type of adsorbent.

Also, the bed length utilized upto the breakthrough point is 20.47 cm at 2 lpm with 298 K for MS-3Å. The maximal bed length of 21.62 cm was utilized in case of activated carbon which is higher than reported for MS-3Å. It can be predicted that effective column efficiency and bed length utilized upto the breakthrough point varies negatively with augmented feed flow rates. The unutilized bed length of MS-3Å is more in comparison to activated carbon. It can be suggested that developed activated carbon performs very well and suitable for CO_2 separation from CO_2/N_2 feed.

The adsorption performance for MS 3Å and AC-SY evaluated as a function of initial adsorbable gas concentrations has been outlined in **Table 5**. The CO_2 uptake varies largely and positively varies with initial concentration of adsorbable gas in feed. The lowest and highest CO_2 uptakes of 7.94 mg/g and 12.31 mg/g were attained for MS-3Å at 2% and 5% CO_2 level, respectively. The maximal CO_2 uptake of 70.13 mg/g was determined for AC-SY compared to a lower value reported for MS-3Å at C_{in}=5% with 298 K and 4 lpm feed flow rate. The lowest Cin= 2 % lpm contributed to a minimal capacity of adsorption and CO_2 uptake of 37.93 mg/g was evaluated for AC-SY. The CO_2 uptake varies proportionally with the initial adsorbable gas level. The adsorption performance of developed activated carbon is reasonably higher at any fixed initial adsorbable gas level in feed. The prepared activated carbon contributed to higher effective column efficiency as evident from the Table 5. Also, the efficiency (η) determined for synthesized carbon is higher and highest η of 0.949 was evaluated at C_{in}= 4% CO_2 level in feed with 4 lpm and 298 K. The highest fraction of total capacity which is effectively used stands at 0.760 for MS-3Å at 3 % CO_2 level with 4 lpm. Notably, the higher efficiency of AC-SY indicates its applicability for economical CO_2 capture. Also, longer bed length L_b was utilized for AC-SY upto the breakthrough point compared to the bed height utilized for MS-3Å for an effective bed length of 23 cm. The maximal bed length of 21.84 cm was utilized in case of AC-SY which is higher than the value obtained for MS-3Å. The developed activated carbon performs satisfactorily in terms of adsorption capacity, column efficiency and utilized bed length as a function of initial CO_2 level.

Table 5 Adsorption performances at different C_{in} levels (T=298 K, F= 4 lpm)

	MS-3Å			AC-SY		
C_{in} (vol.%)	q (mg/g)	η (fr.)	L_b (fr.)	q (mg/g)	η (fr.)	L_b (cm)
2	7.94	0.702	16.15	37.93	0.941	21.65
3	10.93	0.760	17.48	46.95	0.940	19.74
4	12.12	0.758	17.43	61.82	0.949	21.83
5	12.31	0.711	16.35	70.13	0.948	21.84

Mass Transfer Zone

The adsorbable gas amount in solid phase and fluid phase differ as a function of time and the location in the bed. At earliest, the largely CO_2 movement takes place in the vicinity of the column input and feed comes in contact with fresh porous sorbent. The CO_2 concentration in the feed relinquishes drastically with position effectively to zero before the end point of column is reached provided that porous adsorbent has no CO_2 at the start of adsorption. The section of the bed where CO_2 is essentially adsorbed or the section of the bed in which adsorbate amount varies

mostly is widely known as zone of mass transfer (L_{MTZ}). The concentration limits are normally assumed as C_{exit}/C_{in} = 5 to 95% (vol.%). A lean MTZ means the proficient exploitation of the porous adsorbent material leading to reduced regeneration cost of adsorbent. MTZ by and large moves from the input to the outlet all through the process, indicating that the adsorbent adjoining to input achieved the condition of saturation by $CO_{2.}$, after that the zone moves in the direction of the bed's end-side. **Fig.10a-b** demonstrates the narrow and wide mass transfer zones. The steady pattern sorption of CO_2 was assumed for evaluating the L_{MTZ} (Pota and Mathews 1999) utilizing the equation (8):

$$L_{MTZ} = \frac{2\,L(\,t_s - t_b\,)}{t_s + t_b} \qquad (8)$$

The t_s and t_b the exhaustion and breakthrough periods respectively; and L stands for the total bed length. These times correspond to the exit concentrations of 95 % and 5% of C_{in}. The area above the breakthrough curve to the breakthrough period (t_b) denotes the actual amount adsorbed. The breakthrough profile will be rather steep if the L_{MTZ} is thin comparative to the bed length and breakthrough point contributes to the utilization of the nearly all of the capacity. The breakthrough profile very much extended in the situation of L_{MTZ} is approximately equal to column length. The mass transfer zone characterizes by insignificant width assuming no axial dispersion and no resistance of mass transfer. Under such condition, the breakthrough curve possibly remains a vertical line between C_{exit}/C_{in} = 0 and 1.0 when all the adsorbent is saturated. The porous sorbent is wholly saturated between the bed inlet and the start of the L_{MTZ} under the breakthrough condition. The adsorbent under the MTZ goes from nearly saturated to almost no adsorbate, and for a rough average this sorbent material possibly believed to be nearly 50% saturated. For the presumed breakthrough curves as symmetric, the utilisation factor f can be evaluated as:

$$f = 1 - \frac{0.5\,L_{MTZ}}{L} \qquad (9)$$

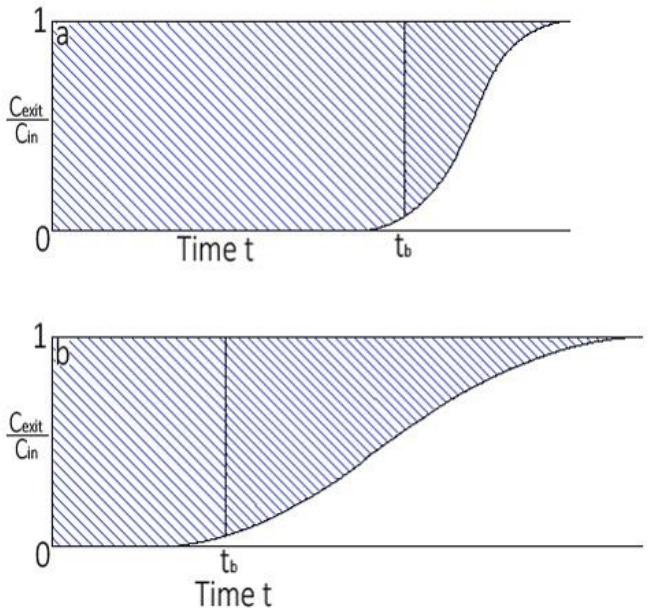

Fig.10 Breakthrough profiles: **(a)** Breakthrough profile and narrow MTZ. **(b)** breakthrough profile and wide MTZ

The parameters of the CO_2 capture, i.e. exhaustion time, breakthrough time, L_{MTZ} and f have been evaluated for MS-3Å and depicted in **Table 6**. The exhaustion and breakthrough times lessen with increased temperatures. The capacity utilization factor varies marginally with increased temperature. Smaller mass transfer zone leads to increased utilization factor. The shortest L_{MTZ} equivalent to 2.28 cm results in good utilization factor of 0.950 at 298 K with F= 3 lpm and C_{in}= 5%. The breakthrough and exhaustion spans reduce with increased feed flow in the range of 2 to 5 lpm. The feed rate variations contribute considerably to L_{MTZ} and f as evident from the findings**.** The L_{MTZ} of 2.28 cm was realized at feed flow rate of 3 lpm with a utilization factor to 0.950 at 298 K and C_{in}=5%. The reduced utilization factor of 0.855 was evaluated at highest studied feed flow of 5 lpm at fixed operating condition of temperature and initial CO_2 level.

The breakthrough period also varies with initial CO_2 level in feed. The utilization factors estimated at different C_{in} do differ notably under constant operating conditions of temperature and feed flow. Overall, the under different operating conditions, smaller L_{MTZ} signifies high utilization factor. The minimal L_{MTZ} equal 2.23 cm for 23 cm effective bed length signifies the utilization of very good bed capacity at breakthrough condition. The highest f= 0.950 was predicted at lowest temperature of 298 K with F= 3 lpm and C_{in} = 5%. The high utilization factor is always considered necessary for economical separation of CO_2 from CO_2/N_2 mixture.

Table 6 Summary of characteristic CO_2 capture parameters of MS-3Å

T(K)	F(slpm)	C_{in}(vol.%)	t_b(s)	t_s(s)	L_{MTZ} (cm)	f
298	4	5	417	513	4.75	0.897
308	4	5	388	459	3.86	0.916
318	4	5	250	335	6.67	0.855
328	4	5	210	283	6.81	0.852
298	2	5	650	803	4.84	0.895
298	3	5	460	593	2.28	0.950
298	5	5	200	268	6.68	0.855
298	4	2	420	598	8.04	0.825
298	4	3	413	543	6.26	0.864
298	4	4	360	475	5.53	0.880

The same characteristics parameters of the CO_2 adsorption calculated for AC-SY have been depicted in Table 7. The exhaustion and breakthrough times diminish with increased temperatures in the range of 298 - 328 K. The shortest L_{MTZ} of 1.20 cm for effective bed length of 23 cm was realized at 298 K leading to increased utilization factor of 0.974 cm with F= 4 lpm and C_{in}=5%. The capacity utilization factor varies negatively with increased temperature and maximal value was reported at a temperature of 298 K. Smaller L_{MTZ} is always desired for efficient separation of CO_2 from feed mixture resulting in increased utilization factor. The breakthrough and exhaustion times

reduce with raised feed flows in the range of 2 to 5 lpm. The feed rate variations contribute marginally to L_{MTZ} and f as evident from the findings**.** The nearly the same L_{MTZ} and f were determined at the feed flow of 2 and 3 lpm with fixed T= 298 and C_{in}=5% and the CO_2 uptake utilization factor of 0.696 was determined at the same feed flows. The exhaustion and breakthrough period also varies with initial CO_2 level in feed. The utilization factors estimated at different C_{in} do differ notably under constant operating conditions of temperature and feed flow. The increased utilization factor equal to 0.974 was attained with L_{MTZ}= 1.20 cm at adsorbable level of 4% with T=298 K and F=4 lpm. Overall, the under different operating conditions, smaller mass transfer zones signifies high utilization factor. The high utilization factor is always desired for economical separation of CO_2 from CO_2/N_2 mixture.

Table 7 Summary of characteristic CO_2 capture parameters of AC-SY

T(K)	Q(slpm)	C_{in}(vol.%)	t_b(s)	t_s(s)	L_{MTZ} (cm)	f
298	4	5	1524	1615	1.33	0.971
308	4	5	1265	1348	1.46	0.968
318	4	5	1059	1138	1.65	0.964
328	4	5	900	958	1.44	0.969
298	2	5	2603	2769	1.42	0.969
298	3	5	1833	1951	1.43	0.969
298	5	5	1401	1494	1.48	0.968
298	4	2	2280	2422	1.39	0.970
298	4	3	1884	2005	1.43	0.969
298	4	4	1875	1975	1.20	0.974

Fig. 11a depicts the profiles of temperature measured by thermocouples T1–T6 for adsorption-desorption process with F= 4 lpm and C_{in}= 5% along the axial positions inside the column. The data were collected for MS-3Å. Temperature of hot-water circulator was preset at 308 K using PID controller. All the temperature sensors (T1-T6) are positioned at different axial locations inside the bed. T6 and T1 correspond to temperatures at extreme bottom and top positions, correspondingly. The T5–T2 denotes intermediary temperatures from the bottom to top direction. Each temperatures sensor is insulated type-K thermocouples with an accuracy of ±0.15 K. The increase in temperature above the preset values (308 K) during the initial adsoption period credited to an exothermic type-adsorption and associated with the liberation of heat. In general, a bed temperature rise of 10 (383 K) to 50 ^oC (323 K) may result when treating vapors with only 1% adsorbable component. The temperature rise is restricted by heat loss for bed of small diameter, but a big adsorber will function approximately adiabatically. Mass transfer forefront is signified by an increased temperature owing to exothermic nature of process and aided by observed profiles at various axial locations. Moreover, with raised concentration of adsorbate, the heat evolved owing to process results in increased temperatures at different locations.

Repeatability measurement was carried out for MS-3Å to ascertain the re-applicability as shown in **Fig.11b**. The coefficient of determination (R^2) and standard deviation (σ) were determined to measure the repeatability. The repeatability measurement was carried out by collecting two sets of data. The data were recorded at a feed flow of 4 lpm with 328 K and C_{in}= 5%. The strong association between the measured data sets was revealed by R^2 =0.994. The mean error of the values (C_{exit}/C_{in}) measured by IR detector was evaluated as ± 0.012 (vol. %). Accuracy and quality of obtained statistics was demonstrated adequately by measuring the repeatability. The determined σ value explains excellent conformity among the measurements. It was suggested that repeatability was agreeable to rely upon the measurement.

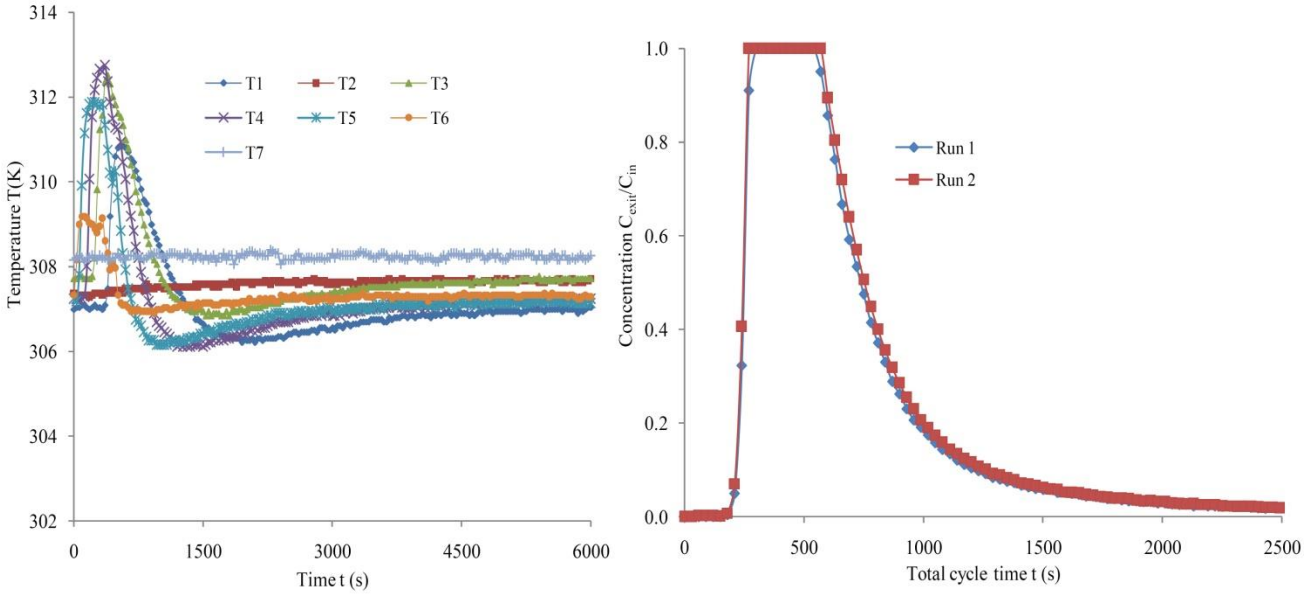

Fig.11 (a) Temperature profiles along axial positions for MS- 3Å at F= 4 slpm and C_{in}= 5%. **(b)** Repeatability assessment utilizing MS-3Å at F= 4 slpm, C_{in}=5% and T=328 K

Conclusions

The dependence of temperature, feed flow and initial CO_2 level on breakthrough and exhaustion periods is very significant and these periods vary considerably with the operating parameters. It was clearly demonstrated that exhaustion and breakthrough spans are longer for produced carbon from date stone compared to that for MS-3Å under different set of operating conditions. The adsorption profiles produced for AC-SY under different operating condition are vastly steep, demonstrating the excellent utilisation of the adsorbent capacity at breakthrough. The maximal CO_2 uptake of 13.83 mg/g was attained at 4 lpm with T=298 K and C_{in}= 5% for MS-3Å. The MS-3Å also contributes to an effective column efficiency of 0.89 with used bed length of 19.44 cm. The highest CO_2 uptake of 73.08 mg/g was evaluated at 5 lpm with T= 298 and C_{in}=5 % for activated carbon. The activated carbon performs very well with high column efficiency of 0.949 and usable bed height equal to L_b=21.84 cm. The MS-3Å is also characterised by L_{MTZ} = 2.28 cm and f value of 0.950 at 3 lpm with T=298 K and C_{in}=5%. The activated carbon

performs better with lessen length of mass transfer zone of 1.20 cm and improved utilization factor of 0.974 at 298 K, C_{in}= 4% and F=4 lpm. It is clearly observed that synthesized carbon from low-cost date stone biomass performs better compared with the MS-3Å. It is suggested that utilizing the date stones for the production of porous carbon is economically realistic to separate CO_2 from the CO_2/N_2 mixture.

Funding The authors thank the Deanship of Scientific research, King Khalid University for grant support (Grant number: R.G.P2/96/41).

Authors' contributions Mohd Danish: data curation, formal analysis, investigation, writing-original draft; Vijay Parthasarthy: conceptualization, methodology, supervision, validation; Mohammed K. Al Mesfer: conceptualization, supervision, writing-review and editing

Data availability The used during the current study are available from corresponding author on reasonable request.

Compliance with ethical standards

Competing Interest Authors declare that there is no competing interest.

Ethics approval and consent to participate Not applicable

Consent to participate Not applicable

Consent for publication Not applicable

References

Al-Janabi N, Vakili R, Kalumpasut P, Gorgojo P, Siperstein FR, Fan X (2018) Velocity variation effect in fixed bed columns: a case study of CO_2 captures using porous solid adsorbents. AIChE J 64: 2189-2197.

Al Mesfer MK (2020). Synthesis and characterization of high-performance activated carbon from walnut shell biomass for CO_2 capture. Environ Sci Pollut Res 27:15020-15028.

Al Mesfer MK, Danish M (2018) Breakthrough adsorption study of activated carbons for CO_2 separation from flue gas. J Environ Chem Eng 6: 4514-4524.

Al Mesfer MK, Danish M, Fahmy MY, Rashid MM (2018) Post combustion CO_2 capture with activated carbons using fixed bed adsorption. Heat Mass Transf 54: 2715-2724.

Alonso M, Rodriguez N, Gonzalez B, Grasa G, Murillo R, Abanades JC (2010) Carbon dioxide capture from combustion flue gases with a calcium oxide chemical loop: Experimental results and process developments. Int J Greenh Cont 4:167-173.

Banat F, Al-Asheh S, Makhadmeh L (2003) Preparation and examination of activated carbons from date pits impregnated with potassium hydroxide for the removal of methylene blue from aqueous solutions. Adsorpt Sci Technol 21(6):597-606.

Belhachemi M, Rios RVRA, Addoun F, Silvestre-Albero J, Sepulveda-Escribano A, Rodrigues-Reinoso F (2009) Preparation of activated carbon from date pits: effects of agents and liquid phase oxidation. J Anal Appl Pyrosis 86:168-172.

454 Calvo-Munoz EM, Garcia-Mateos FJ, Rosas, Rodrigues-Mirasol J, Cordero T (2016) Biomass waste carbon materials as
455 adsorbents for CO_2 capture under post-combustion conditions. Front Mater 3:1-14.

456 Cohen SM, Chalmers HL, Webbe ME, King CW (2011) Comparing post-combustion carbon dioxide capture operation at
457 retrofitted coal-fired power plants in the Texas and Great Britain electric grids. Environ Res Lett 6:1-14.

458 Coromina HM, Walsh DA, Mokaya R (2016) Biomass-derived activated carbon with simultaneously enhanced CO_2 uptake
459 for both pre and post combustion capture applications. J Mater Chem A 4:280-289.

460 Daniel VV, Gulyani BB, Kumar BGP (2012) Usage of date stones as adsorbents: A review. J Disper Sci Technol 33:1321-
461 1331.

462 Davis E, Kopac J (2014) Activated carbons derived from residual biomass pyrolysis and their CO_2 adsorption capacity. J
463 Anal Appl Pyrol 110:322-332.

464 Dejang N, Somprasit O, Chindaruksa S (2015) Preparations of activated carbon from Macadamia shell by microwave
465 irradiation activation. Energy Procedia 79:727-732.

466 Garcia S, Gil MV, Martin CF, Pis JJ, Rubiera F, Pevida C (2011) Breakthrough adsorption study of a commercial activated
467 carbon for pre-combustion carbon dioxide capture. Chem Eng J 171:549-556.

468 Hao W, Bjorkman E, Lilliestrale M, Hedin N (2013) Activated carbon prepared from hydrothermally carbonized waste
469 biomass used as adsorbent for CO_2. Appl Energy 112: 526-532.

470 Hong S, Jang E, Dysart D, Pol VG, Lee KB (2016) CO_2 capture in the sustainable wheat-derive activated microporous
471 carbon compartments. Sci Rep 6:1-10.

472 Jahangiri M, Shahtaheri SJ, Adl J, Rashidi A, Kakooei H, Forushani AR, Nasiri G, Ghorbanali A (2012) Preparation of
473 activated carbon from walnut shell and its utilization for manufacturing organic-vapor respirator cartridge. Fresenius
474 Environ Bull 21:1508-1514.

475 Lewicka K (2017) Activated carbons prepared from hazelnut shells, walnut shells and peanut shells for high CO_2
476 adsorption. Pol J Chem Technol 19:38-43.

477 Lira-Zuniga S, Saez-Navarrete C, Rodrigues-Cordova L, Herrera-Zeppelin L, Herrera-Urbina R (2016) CO_2 adsorption on
478 agricultural biomass combustion ashes. Maderas-Cienc Technol. 18, 607-616.

479 Lu C, Bai B, Wu B, Su F, Hwang JF (2008) Comparative study of CO_2 capture by carbon nanotubes, activated carbons, and
480 zeolites. Energy Fuels 22: 3050-3056.

481 MacDowell N, Florin N, Buchard A, Hallett J, Galindo A, Jackson G, Adjman C, Williams CK, Shah N, Fennel P (2010)
482 An overview of carbon dioxide captures technologies. Energy Environ Sci 3:1645-1669.

483 Mataji M, Khoshandam B (2014) Benzene adsorption on activated carbon from walnut shell. Chem Eng Comm 201:1294-
484 1313.

485 Monazam ER, Spenik J, Shadle LJ (2013) Fluid bed adsorption of carbon dioxide on immobilized polyethylenimine (PEI):
486 kinetic analysis and breakthrough behaviour. Chem Eng J 223:795-805.

487 Ogungbenro AE, Quang DV, Al-Ali K, Abu-Zahra, MRM (2017) Activated carbon from date seeds for CO_2 capture
488 applications. Energy Procedia 114: 2313-2321.

Patil P, Singh S, Kumar YM (2013) Preparation and study of properties of activated carbons produced from agricultural and industrial waste shells. Res J Chem Sci 3:12-15.

Peredo-Mancilla D, Hort C, Ghimbeu CM, Jeguirim M, Bessieres D (2018) CO_2 and CH_4 adsorption behaviour of Biomass-based activated carbons. Energies 22:1-12.

Plaza MG, Pevida C, Arias B, Fermoso J, Casal MD, Martin CF, Rubiera F, Pis JJ (2019) Development of low-cost biomass-based adsorbents for postcombustion CO_2 capture. Fuel 88: 2442-2447.

Pota AA, Mathews AP (1999) Effect of particle stratification on fixed bed adsorber performance. J Environ Eng 8:705-711.

Rashidi NA, Yusuf S (2016) An overview of activated carbons utilization for the post combustion carbon dioxide captures. J CO_2 Util 13:1-16.

Serafin J, Narkiewicz U, Moraeski AW, Wrobel RJ (2017) Highly microporous activated carbons from biomass for CO_2 capture and effective micropores at different conditions. J CO_2 Util 18:73-79.

Serna-Guerrero R, Sayari A (2010) Modeling adsorption of CO_2 on amine functionalized mesoporous silica. 2: kinetics and breakthrough curve. Chem Eng J 161:182-190.

Shahkarami S, Azargohar R, Dalai AK, Soltan J (2015) Breakthrough CO_2 adsorption in bio-based activated carbons. J Environ Sci 34: 68-76.

Shen C, Grande CA, Li P, Yu J, Rodrigues AE (2010) Adsorption equilibria and kinetics of CO_2 and N_2 on activated carbon beads. Ind Eng Chem Res 47: 4883-4890.

Shen C, Yu J, Li P, Grande CA, Rodrigues AE (2011) Capture of CO_2 from flue gas by vacuum pressure swing adsorption using activated carbon beads. Adsorption 17: 179-188.

Toprak A, Kopac T (2017) Carbon dioxide adsorption using high surface area activated carbons from local coals modified by KOH, NaOH and $ZnCl_2$ agents. Int J Chem React Eng 15:1-16.

Valverde JM, Pontiga F, Soria-Hoyo C, Quintanlla MAS, Moreno H, Duran FJ, Espin MJ (2011) Improving the gas solids contact efficiency in a fluidized bed of carbon dioxide adsorbent fine particles. Phys Chem Chem Phys 13:14906-14909.

Xia H, Cheng S, Zhang L, Peng J (2016) Utilization of walnut shell as a feedstock for preparing high surface area activated carbon by microwave induced activation: effect of activation agents. Green Process Synthesis 5:1-2.

Yang H, Xu Z, Fan M, Gupta R, Slimane RB, Bland AE, Wright I (2008) Progress in carbon dioxide separation and capture: a review. J Environ Sci 20:14-27.

Zeng G, Lou S, Ying H, Wu X, Dou X, Ai N, Wang J (2018) Preparation of microporous carbon from sargassum horneri by hydrothermal carbonization and KOH activation for CO_2 capture. J Chem. 1-9.

Zhang C, Song W, Ma Q, Xie L, Zhang X, Guo H (2016) Enhancement of CO_2 capture on biomass-based carbon from black locust by KOH activation and ammonia modification. Energy Fuel 305:4181-4190.

List of Figures with captions:

List of tables with captions:

Figures

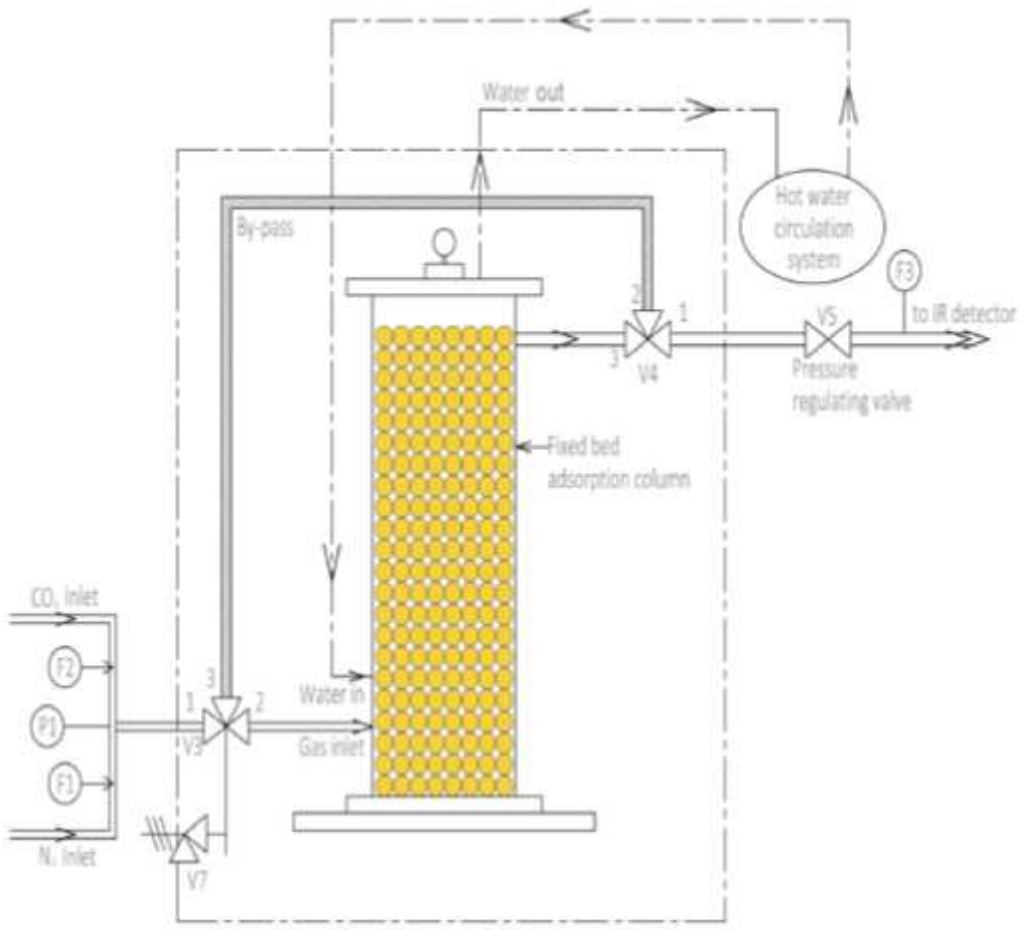

Figure 1

Fixed bed column

Figure 2

Date stone based biomass and activated carbon: (a) MS 3Å. (b) Date stone after oven drying. (c) Activated carbon AC-SY

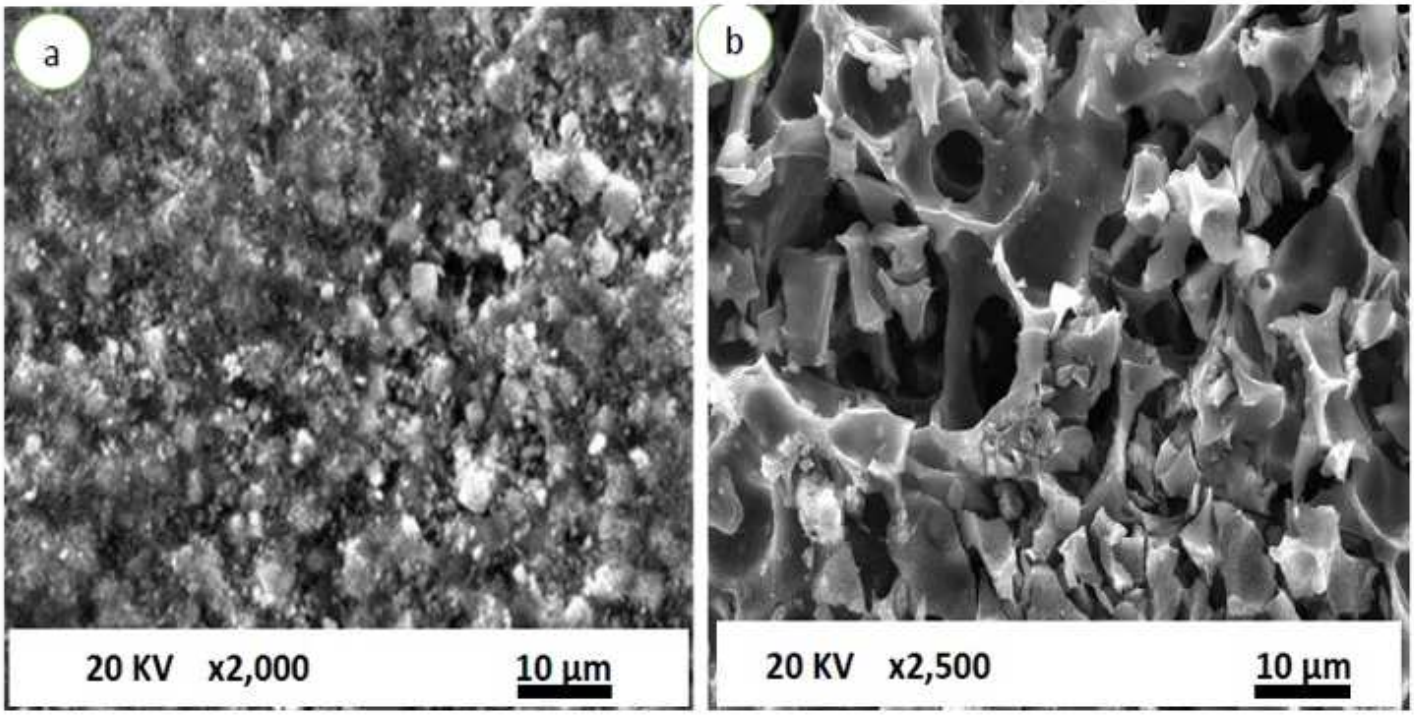

Figure 3

Morphological characteristics of adsorbents used for CO2 capture: (a) MS-3Å (b) AC-SY

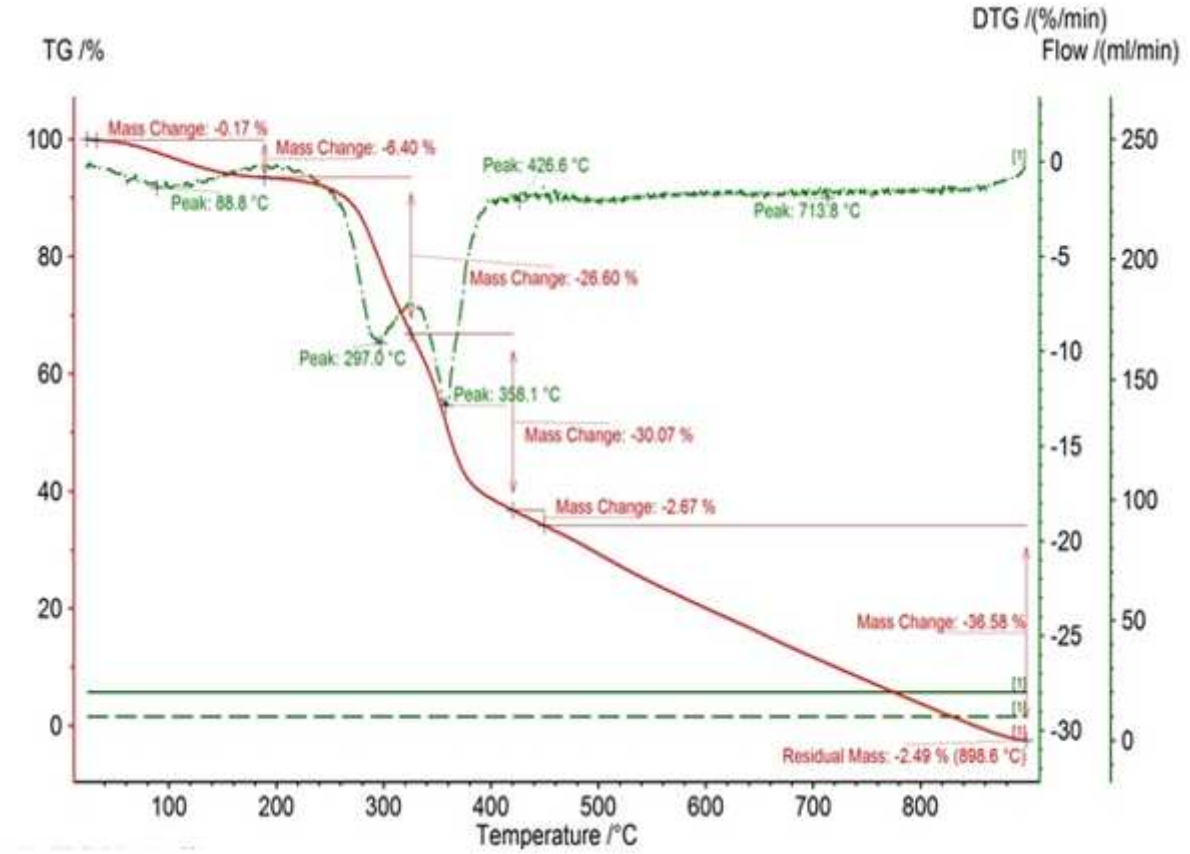

Figure 4

Thermogravimetric analysis curve of DS showing mass change and DGT

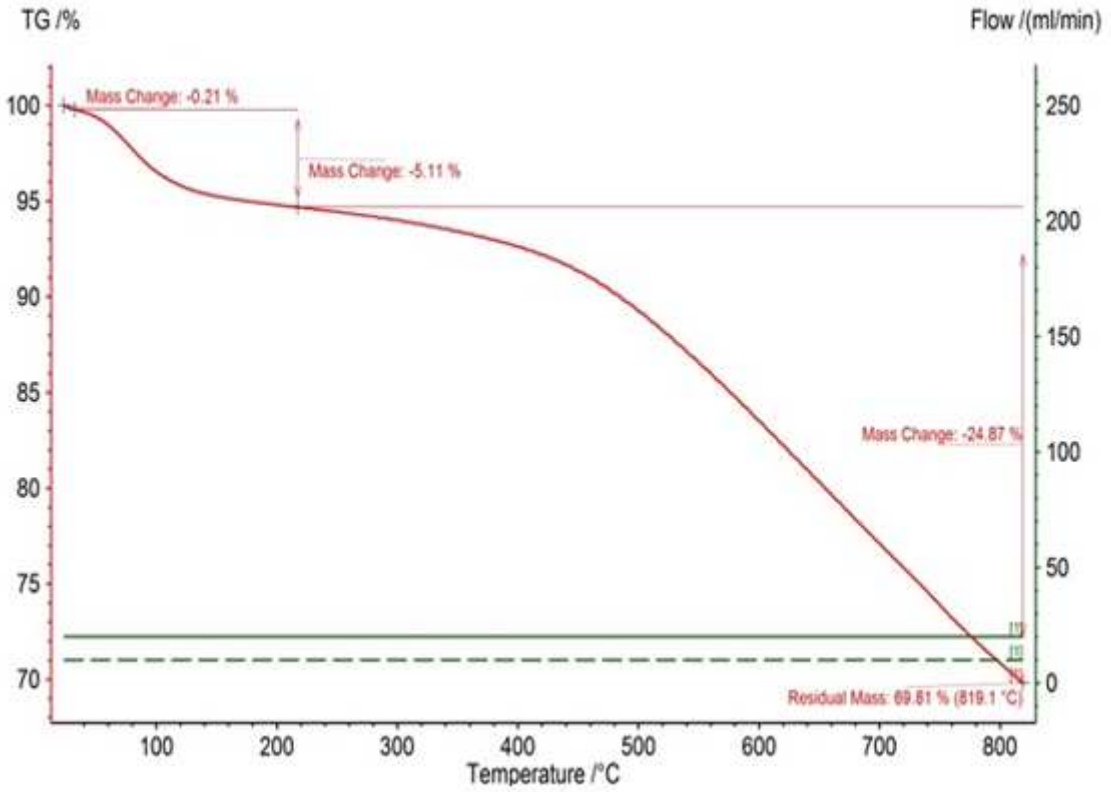

Figure 5

Thermogravimetric analysis curve of AC-SY showing mass change

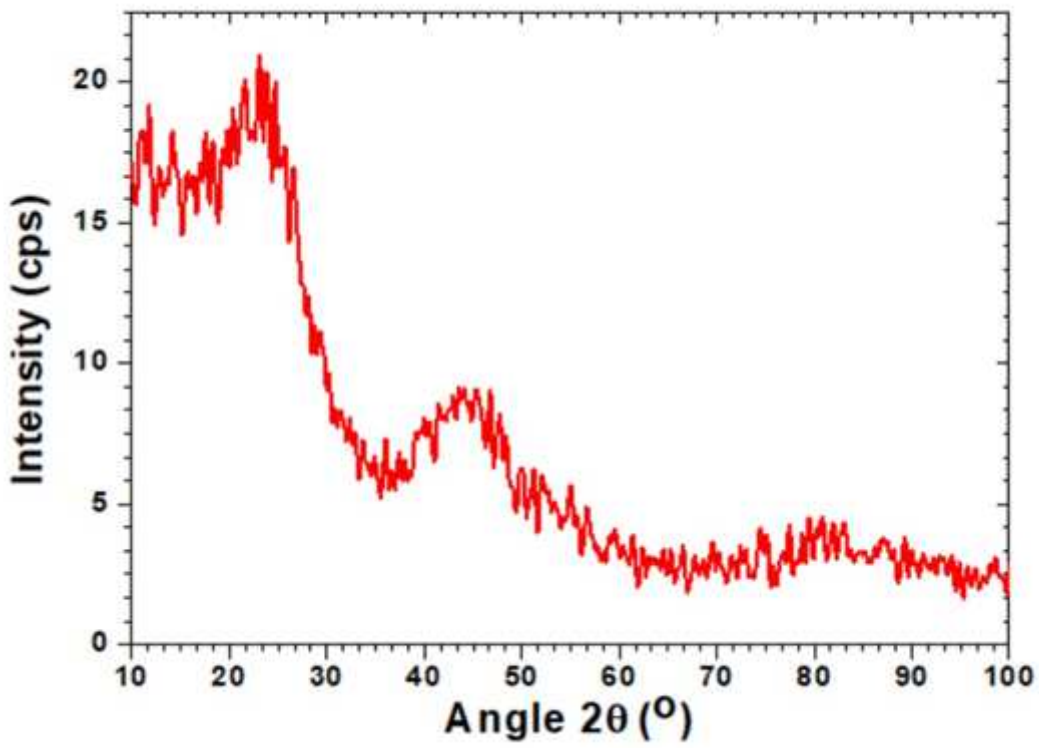

Figure 6

XRD analysis of date stone based activated carbon AC-SY

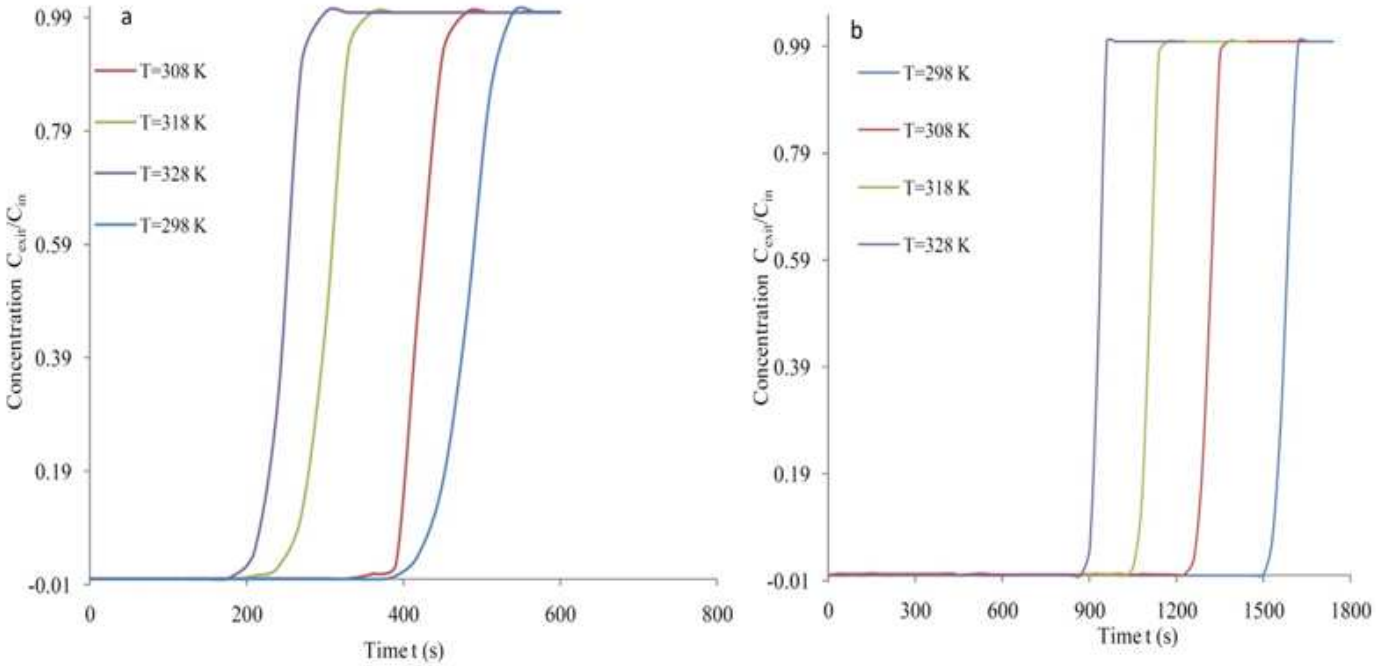

Figure 7

Adsorption response at various temperatures at F= 4 lpm, Co=5%, (a) MS 3Å. (b) AC-SY

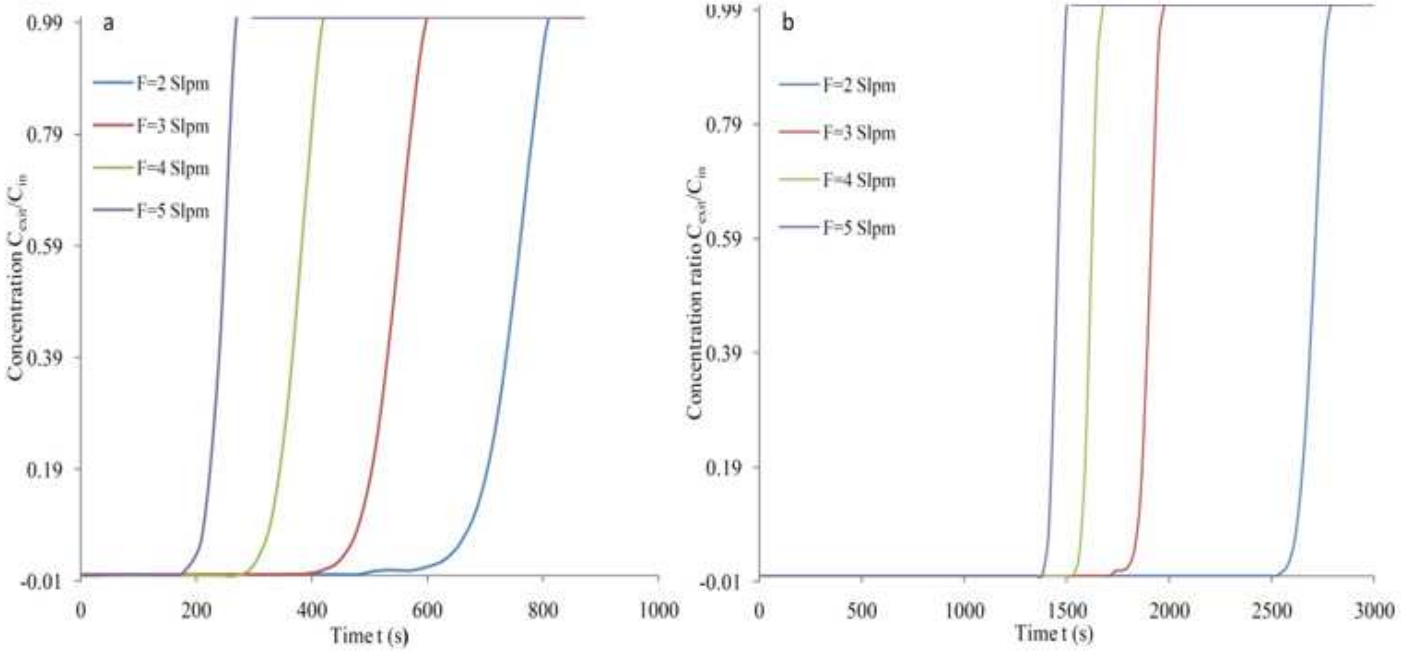

Figure 8

Adsorption response at various feed rates at T= 298 K, Cin=5%, (a) MS-3Å. (b) AC-SY

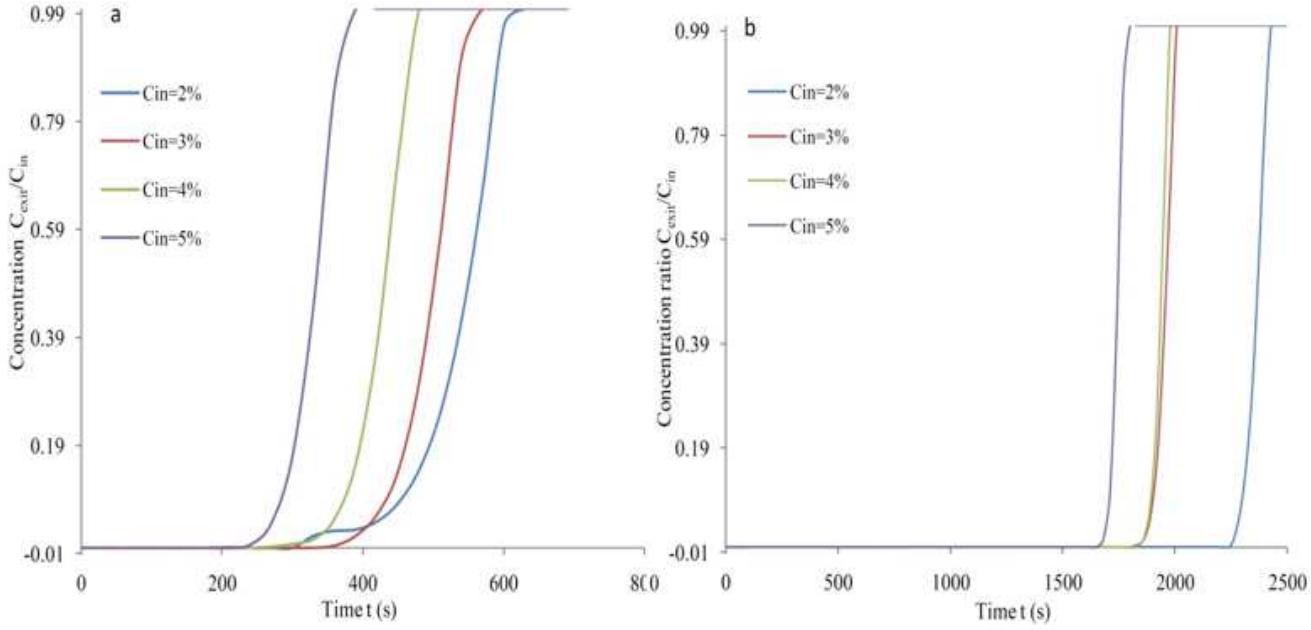

Figure 9

Adsorption response at various CO2 level at F= 4 L/min, T= 298K, (a) MS-3Å. (b) AC-SY

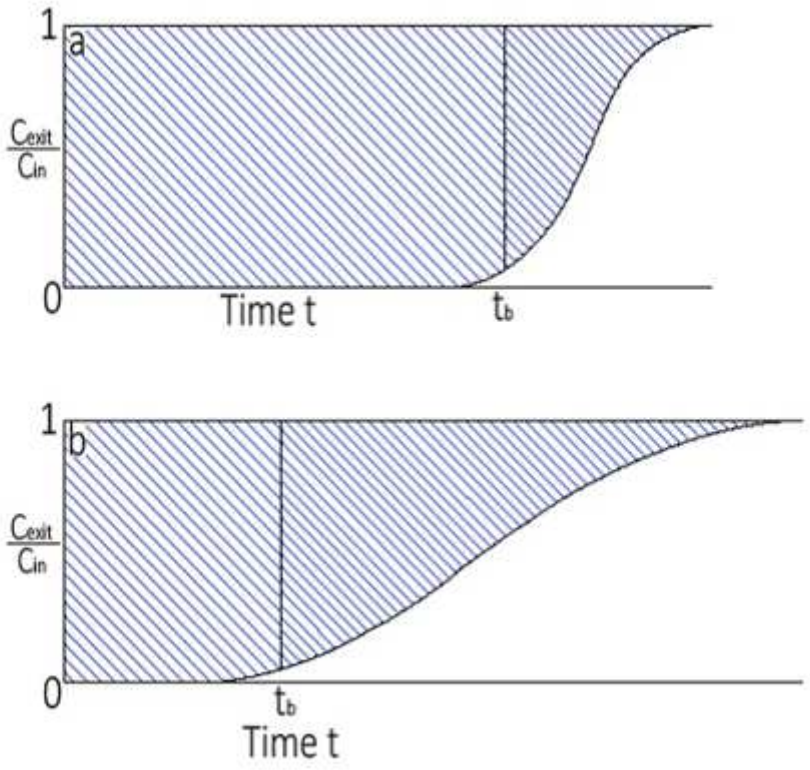

Figure 10

Breakthrough profiles: (a) Breakthrough profile and narrow MTZ. (b) breakthrough profile and wide MTZ

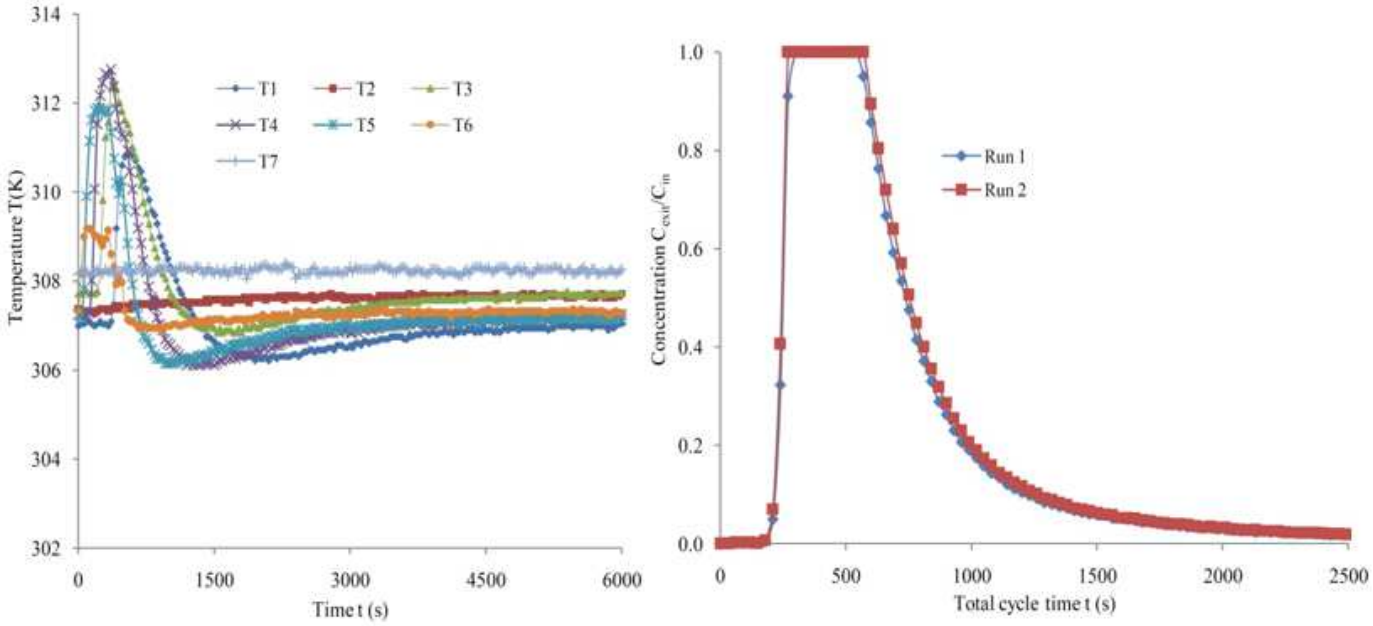

Figure 11

(a) Temperature profiles along axial positions for MS- 3Å at F= 4 slpm and Cin= 5%. (b) Repeatability assessment utilizing MS-3Å at F= 4 slpm, Cin=5% and T=328 K